IEEE Access
Multidisciplinary | Rapid Review | Open Access Journal

Received 30 November 2022, accepted 28 December 2022, date of publication 2 January 2023, date of current version 5 January 2023.

Digital Object Identifier 10.1109/ACCESS.2022.3233645

RESEARCH ARTICLE

Optimal Array Phase Center Study for Frequency-Domain Constrained Space-Time Broadband Beamforming

YANG WANG, HAIYUN XU, BIN WANG, AND MINGLEI SUN
PLA Strategic Support Force Information Engineering University, Zhengzhou 450001, China
Corresponding author: Bin Wang (commutech@163.com)

ABSTRACT The frequency-domain constrained broadband space-time beamformer has been widely used in many fields because of its excellent performance and no need for pre-steering delay. However, the beam response of the frequency-domain constrained space-time broadband beamformer depends heavily on the phase center location of the array. The wrong phase center location of the array will lead to undesirable wide main lobe and high side lobe. To choose the location of the phase center of the array correctly, this paper makes an in-depth theoretical discussion on this dependency based on the uniform linear array. First, the dependence of the quiescent beam response of the frequency-domain constrained space-time broadband beamformer on the phase center location of the array is theoretically derived, and it is proved that there is an optimal phase center location of the array which can make the beamformer obtain the best quiescent beam response. Then, a selection criterion of the optimal array phase center location is proposed, and based on this criterion, the closed-form solution of the optimal array phase center location is theoretically derived when the constraint matrix contains two pre-selected points. Finally, based on the closed-form solution, through correct extrapolation, the suboptimal solution for the optimal array phase center location is obtained when the constraint matrix contains any preselected points. Numerical simulations verify the correctness and effectiveness of the proposed methods.

INDEX TERMS Quiescent beam response, array phase center, space-time broadband beamformer, frequency-domain constraints.

I. INTRODUCTION

Broadband beamforming has been an important research topic over the past few decades, and its applications cover many different fields, such as sonar, radar, wireless communications, microphone arrays, and medical imaging [1], [2], [3], [4], [5].

According to the choice of weights, broadband beamforming can be classified as data-independent and statistically optimum [6], [7]. The weight solution of the data-independent broadband beamformer is independent of array data, and the desired azimuth/frequency response is designed by a linear constraint method or a pattern synthesis method [8], [9], [10], [11], [12]. The weight selection of the statistically optimum broadband beamformer is to optimize the array response based on statistics of the array data [13], [14], [15], [16], [17], [18], [19], [20], [21], [22]. The array statistics are usually unknown and time-varying, so adaptive algorithms are usually used to update the weights. In addition, the design technology of data-independent beamformer is typically applied to statistically optimum beamforming.

According to whether array data is processed in frequency-domain or time-domain broadband beamforming methods can be divided into two categories, namely, the space-frequency method based on discrete Fourier transform (DFT) and the space-time method based on finite impulse response (FIR). The space-frequency method divides the time-domain array data into frequency-domain data of multiple sub-bands

The associate editor coordinating the review of this manuscript and approving it for publication was Manuel Rosa-Zurera.

by DFT. DFT can reduce the correlation between frequency domain data in different frequency sub-bands. Frequency-domain narrowband beamforming can be performed in each sub-band under the condition that the frequency range of each sub-band satisfies the narrowband requirement [12], [13], [14]. After obtaining all the output data from the narrowband beamformer, the DFT-based beamformer converts the frequency-domain output data into the time-domain output through the inverse discrete Fourier transform (IDFT) processor. However, DFT-based space-frequency methods usually need many data samples to meet the narrowband conditions [15].

The FIR-based space-time method adds tapped delay lines after each array element. It uses a linear constrained minimum variance method to control the gain of the beamformer on the desired broadband signal, while suppressing other interference signals [16], [17], [18], [19], [20]. The Frost beamformer is the most classical space-time broadband beamformer (STBB) [16]. The linear constraint of STBB requires that the phase of the desired signal is consistent at the output of each array element, so the beamformer needs to pre-steer the array data in advance. Moreover, the Frost beamformer requires that the pre-steering delay must have very high delay accuracy, otherwise the delay error may cause the desired signal to be mistakenly suppressed as interference [21]. In order to eliminate the delay of pre-steering, some new linear constraint design methods are proposed. Buckley proposed the real data point constraint (RDPC) [22], which controls the gain of the single-tone cosine function by designing linear constraints, so as to achieve gain control of the desired signal. The RDPC completes the design and execution of linear constraints directly in the time-domain. Gadara proposed the Convolution Constraints (CC) [23], which design linear constraints in the frequency-domain and implement linear constraints in the time-domain by convolution operation. However, the length of the tapped delay line in the CC determines the frequency of the preselected points. Reducing the frequency interval of the preselected points must increase the length of the tapped delay line, which increases the computational complexity of the algorithm. Then Ebrahimi proposed the frequency-domain constraints (FC) [24]. It can realize the linear constraints designed in the frequency-domain with low complexity in the time-domain, and can arbitrarily select the frequency of the preselected points without changing the length of the tapped delay line.

The quiescent beam response refers to the optimal beam response when the input of the array contains only white noise [8], which determines the initial state of the adaptive array beam response. The resulting array weight vector is called quiescent solution. The quiescent solution of the space-time broadband beamformer is determined by the geometric shape of the array and the design of the linear constraints. It has been proved in [25], [26], [27], and [28] that when the linear constraint is the derivative constraint, the quiescent beam response depends on the array phase center. Buckley has studied the influence of this dependence on the beam response of a generalized sidelobe canceller [26], and at the same time, it has eliminated this influence by finding the phase center of the array that minimizes the output power of the array under white noise conditions. However, when the linear constraint is the frequency-domain constraint, the dependence of the quiescent beam response on the phase center of the array has not been thoroughly studied, and even its existence has not been pointed out.

In this paper, in order to solve the problem of selecting the optimal phase center location of the array of the frequency-domain constrained space-time broadband beamforming (FCSTBB), the dependence of its quiescent beam response on the array phase center is deeply studied. First, we point out that the quiescent beam response of the FCSTBB depends on the phase center of the array, and the accuracy of this dependence is verified by theoretical derivation and numerical simulation. Then, minimizing the quiescent output power of the array under white noise input is selected as the selection criterion of the optimal phase center location of the array. On this basis, the closed-form solution of the optimal phase center location of the array is theoretically derived when the constraint matrix contains two preselected points. The closed-form solution can make the quiescent beam response of the beamformer obtain the narrowest main lobe width and the lowest side lobe level. Finally, since the inverse of the matrix exceeding the second order can not be expanded, the closed-form solution of the optimal phase center location of the array can not be solved when the constraint matrix contains more than two preselected points. Based on the closed-form solution of the optimal phase center location of the array when the constraint matrix contains two preselected points, we correctly extrapolate the suboptimal solution for the optimal phase center location when the constraint matrix contains any number of preselected points.

The main contributions of this paper are summarized as follows:

1) The dependence of the quiescent beam response of FCSSTBB on the location of the phase center of the array is derived theoretically.
2) The closed-form solution of the optimal array phase center location of FCSTBB is theoretically derived when the constraint matrix contains two pre-selected points. This solution can achieve the narrowest main lobe width and the lowest sidelobe level in the quiescent beam response of the beamformer.
3) The sub-optimal solution of the beamformer is correctly extrapolated when the constraint matrix contains any number of preselected points.

The structure of this article is as follows. Section II briefly introduces space-time broadband beamforming and frequency-domain constraints. Section III introduces the dependence of quiescent beam response on the phase center of the array. The closed-form solution and the extrapolated suboptimal solution are given in section IV. Section V

provides the simulation results and analysis. At last, the conclusion is given in section VI.

Symbols: Bold characters represent vectors or matrices. $[\cdot]^{\mathrm{T}}$ and $[\cdot]^{\mathrm{H}}$ represent the transpose and conjugate transpose of a matrix or vector, respectively. $\mathrm{E}\{\cdot\}$ denotes the statistical expectation. $\Phi(\cdot)$ means the phase. $|\cdot|$ represents the modulus. $\otimes$ marks the Kronecker product.

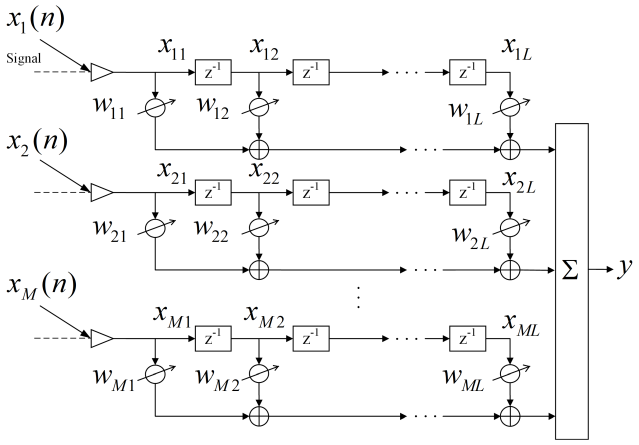

FIGURE 1. The basic array structure of the space-time broadband beamformer without pre-steering delays.

II. PROBLEM BACKGROUND

A. SPACE-TIME BROADBAND BEAMFORMING

Considering a uniform linear array (ULA) consisting of M omnidirectional sensors, a tapped delay line of length L is connected after each sensor. Fig. 1 shows the basic array structure of the STBB without pre-steering delays [24]. The input data of the sensor channel at the n-th data sample is $x_1(n), x_2(n), \ldots, x_M(n)$. x_{ml} is the input data of each tap, w_{ml} is the weight coefficient of each tap, where $\mathrm{m} = 1, 2, \ldots, M, l = 1, 2, \ldots, L$. The output of the beamformer can be expressed as

$$y = \sum_{m=1}^{M} \sum_{l=1}^{L} w_{ml} x_{ml} \tag{1}$$

represented in vector form as

$$y = \boldsymbol{w}^H \boldsymbol{x} \tag{2}$$

where

$$\boldsymbol{w} = [w_{11}, \ldots, w_{1L}, w_{21}, \ldots, w_{2L}, \ldots, w_{M1}, \ldots, w_{ML}]^T \tag{3}$$

is the ML-dimensional weight coefficient vector.

$$\boldsymbol{x} = [x_{11}, \ldots, x_{1L}, x_{21}, \ldots, x_{2L}, \ldots, x_{M1}, \ldots, x_{ML}]^T \tag{4}$$

is the ML-dimensional input data vector. For the case that the array data is generalized stationary in time, the equation of the optimal weight vector can be expressed by the beamformer data covariance matrix $R_{xx} = E\left\{x(n)\, x^T(n)\right\}$.

The optimal weight of a space-time broadband beamformer can be found by the following linear constrained minimum variance problem

$$\begin{cases} \min\ \boldsymbol{w}^H \boldsymbol{R}_{xx} \boldsymbol{w} \\ s.t.\ \boldsymbol{C}^H \boldsymbol{w} = \boldsymbol{F} \end{cases} \tag{5}$$

where matrix $\boldsymbol{C}$ and vector $\boldsymbol{F}$ are the $KL \times J$ dimensional constraint matrix and the J-dimensional response vector, respectively. Each column in constraint matrix $\boldsymbol{C}$ imposes a constraint on the weight vector $\boldsymbol{w}$, which is termed stacked constraint vector. The optimal weight vector satisfying (5) is given by

$$\boldsymbol{w}_{opt} = \boldsymbol{R}_{xx}^{-1} \boldsymbol{C} \left(\boldsymbol{C}^H \boldsymbol{R}_{xx}^{-1} \boldsymbol{C} \right)^{-1} \boldsymbol{F} \tag{6}$$

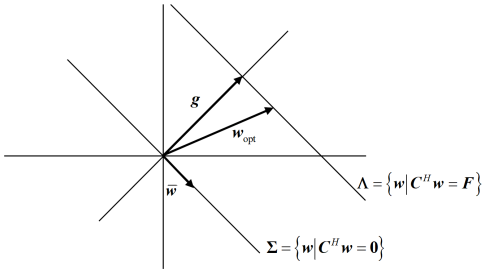

FIGURE 2. ML-dimensional source observation and weight vector space.

As shown in Fig. 2, the optimal weight vector $\boldsymbol{w}_{opt}$ can be orthogonally decomposed into a data-independent quiescent (white noise data) solution vector $\boldsymbol{g}$ and a data-dependent solution vector $\bar{w}$ [16], [22], [25].

where the constraint hyperplane $\boldsymbol{\Lambda}$ composed of all ML-dimensional vectors satisfying the constraint is defined as

$$\boldsymbol{\Lambda} = \left\{ \boldsymbol{w} | \boldsymbol{C}^H \boldsymbol{w} = \boldsymbol{F} \right\} \tag{7}$$

the constraint subspace $\boldsymbol{\Sigma}$ orthogonal to all stacked constraint vectors is defined as

$$\boldsymbol{\Sigma} = \left\{ \boldsymbol{w} | \boldsymbol{C}^H \boldsymbol{w} = \boldsymbol{0} \right\} \tag{8}$$

The quiescent solution vector $\boldsymbol{g}$ is perpendicular to and terminates in the constraint hyperplane $\boldsymbol{\Lambda}$, so it is a linear combination of stacked constraint vectors and satisfies the constraint conditions. The unique expression for the quiescent solution vector $\boldsymbol{g}$ can be expressed as [16]

$$\boldsymbol{g} = \boldsymbol{C} \left(\boldsymbol{C}^H \boldsymbol{C} \right)^{-1} \boldsymbol{F} \tag{9}$$

The quiescent solution vector $\boldsymbol{g}$ is equivalent to the optimal weight vector when the data covariance matrix is proportional to the unit matrix. Therefore, when the input is white noise, $\boldsymbol{g}^H \boldsymbol{x}$ is the optimal response output of the array, and its corresponding beam response is the quiescent beam response. The quiescent solution vector $\boldsymbol{g}$ not only controls the unit gain response of the beamformer to the preselected points, but also controls the main lobe width and sidelobe level of the beam response.

The solution vector $\bar{\boldsymbol{w}}$ is a function of the data covariance matrix R_{xx}, which is orthogonal to all stacked constraint vectors. Substituting the two orthogonal decomposed optimal weight vectors into (2) to obtain the final array beam output

$$y = \boldsymbol{g}^H \boldsymbol{x} + \bar{\boldsymbol{w}}^H \boldsymbol{x} \tag{10}$$

B. FREQUENCY-DOMAIN CONSTRAINTS

Frequency-domain constraint refers to the gain of control over a set of preselected points (representing the direction and frequency of the desired signal) in the frequency domain. A stacked constraint vector in the constraint matrix $\boldsymbol{C}$ can only achieve one preselected point gain control. Stack constraint vector $\boldsymbol{a}\left(\theta_p, f_q\right)$ based on frequency-domain constraint is defined as

$$\boldsymbol{a}\left(\theta_p, f_q\right) = \boldsymbol{S}_t\left(f_q\right) \otimes \boldsymbol{S}_s\left(\theta_p, f_q\right) \tag{11}$$

where $\theta_p\ (p = 1, 2, \ldots, P)$ denotes the direction of the preselected point, $f_q\ (q = 1, 2, \ldots, Q)$ denotes the frequency of the preselected point. $\boldsymbol{a}\left(\theta_p, f_q\right)$ is also referred to as the space-time steering vector of the preselected point. The L-dimensional frequency steering vector $\boldsymbol{S}_t\left(f_q\right)$ can be written as

$$\boldsymbol{S}_t\left(f_q\right) = \left[1, e^{-j2\pi f_q T_s}, \cdots, e^{-j2\pi f_q (L-1) T_s}\right]^T \tag{12}$$

where j is the imaginary unit, T_s is the sampling interval of the data sample. The frequency steering vector can transform the weight coefficient from the time domain to the frequency domain. The M-dimensional space steering vector $\boldsymbol{S}_s\left(\theta_p, f_q\right)$ is expressed as

$$\boldsymbol{S}_s\left(\theta_p, f_q\right) = \left[e^{-j2\pi f_q \tau_{1,\theta_p}}, e^{-j2\pi f_q \tau_{2,\theta_p}}, \cdots, e^{-j2\pi f_q \tau_{M,\theta_p}}\right]^T \tag{13}$$

where τ_{m,θ_p} represents the propagation delay between the m-th sensor and the array phase center when the source direction is θ_p. The space steering vector can compensate for the phase of the weight coefficient that has been transformed to the frequency domain.

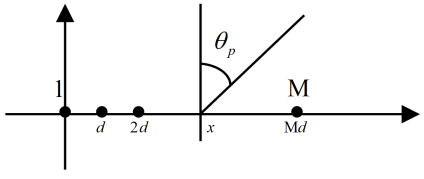

FIGURE 3. Coordinate distribution of uniform linear array.

The coordinate distribution of the ULA is shown in Fig. 3, with the origin of the coordinates located at the location of the first array element and one coordinate axis coinciding with the line where the sensor is located. Let x be the coordinate of the array phase center, then the propagation delay of the source impacted from the azimuth angle θ_p can be constructed as

$$\tau_{m,\theta} = -\left[(m-1)\, d - x\right] \frac{\sin\theta_p}{c} \quad (m = 1, 2, \ldots, M) \tag{14}$$

where d is the distance between two adjacent elements of the ULA, and c is the propagation velocity of the wave.

In space-time broadband beamforming, it is usually necessary to control the gain over the entire desired frequency band in the desired direction. Suppose the desired direction is θ_p. The desired frequency band is decomposed into Q frequency bins, $f_q \in [f_l, f_h]$, $q = 1, 2, \ldots, Q$, f_l and f_h represent the minimum and maximum endpoints of the signal bandwidth, respectively. Considering the weight coefficient is a complex number, the constraint matrix $\boldsymbol{C}$ for achieving preselected point gain control can be expressed as

$$\boldsymbol{C} = \left[\boldsymbol{a}\left(\theta_p, f_1\right), \boldsymbol{a}\left(\theta_p, f_2\right), \ldots, \boldsymbol{a}\left(\theta_p, f_Q\right)\right] \tag{15}$$

the corresponding response vector $\boldsymbol{F}$ is given by

$$\boldsymbol{F} = [1, 1, \ldots, 1]^T \tag{16}$$

III. DEPENDENCE OF BEAM RESPONSE ON ARRAY PHASE CENTER

Regarding the dependence of the beam response on the array phase center for FCSTBB, the following proposition is given in this paper.

Proposition 1: The quiescent beam response of FCSTBB depends on the phase center location of the array.

Proof: The mathematical expression of the quiescent beam response power of FCSTBB is can be calculated as

$$P(\theta, f) = \left|\boldsymbol{F}^H \left(\boldsymbol{C}^H \boldsymbol{C}\right)^{-1} \boldsymbol{C}^H \boldsymbol{a}(\theta, f)\right|^2 \tag{17}$$

where the constraint matrix $\boldsymbol{C}$ and the response vector $\boldsymbol{F}$ are given by (15) and (16), respectively. θ representing direction and f representing frequency. Let $\boldsymbol{V} = \left(\boldsymbol{C}^H \boldsymbol{C}\right)^{-1} \boldsymbol{F}$, which is a Q-dimensional complex vector. Substitute (15)(16) into (17) and expand to obtain

$$P(\theta, f) = \left|\sum_{q=1}^{Q} V_q \boldsymbol{a}^H\left(\theta_p, f_q\right) \boldsymbol{a}(\theta, f)\right|^2 \tag{18}$$

where V_q denotes the q-th element of the complex vector $\boldsymbol{V}$. Joint (11) (12) (13) (14) expansion calculation $\boldsymbol{a}^H\left(\theta_p, f_q\right) \boldsymbol{a}(\theta, f)$ get

$$\begin{aligned} &\boldsymbol{a}^H\left(\theta_p, f_q\right) \boldsymbol{a}(\theta, f) \\ &= \left[\boldsymbol{S}_t\left(f_q\right) \otimes \boldsymbol{S}_s\left(\theta_p, f_q\right)\right]^H \left[\boldsymbol{S}_t(f) \otimes \boldsymbol{S}_s(\theta, f)\right] \\ &= \left[\boldsymbol{S}_t^H\left(f_q\right) \boldsymbol{S}_t(f)\right] \otimes \left[\boldsymbol{S}_s^H\left(\theta_p, f_q\right) \boldsymbol{S}_s(\theta, f)\right] \\ &= \frac{\sin(L\varphi_t/2)}{\sin(\varphi_t/2)} \frac{\sin(M\varphi_s/2)}{\sin(\varphi_s/2)} e^{-j\left(\frac{L-1}{2}\varphi_t + \varphi_0 + \frac{M-1}{2}\varphi_s\right)} \end{aligned} \tag{19}$$

where

$$\begin{cases} \varphi_t = 2\pi T_s\left(f - f_q\right) \\ \varphi_0 = -\dfrac{2\pi x}{c}\left(f \sin\theta - f_q \sin\theta_p\right) \\ \varphi_s = \dfrac{2\pi d}{c}\left(f \sin\theta - f_q \sin\theta_p\right) \end{cases} \tag{20}$$

The modulus of $\boldsymbol{a}^H\left(\theta_p, f_q\right)\boldsymbol{a}\left(\theta, f\right)$ is independent of array phase center x but its phase function depends on array phase center x. The phase difference $\Delta_{u,v}$ between $\boldsymbol{a}^H\left(\theta_p, f_q\right)\boldsymbol{a}\left(\theta, f\right)$ for different preselected frequencies f_u, f_v can be calculated as

$$\begin{aligned}&\Delta_{u,v}\\&\quad=\left(f_u-f_v\right)\\&\qquad\times\left[\pi T_s\left(L-1\right)-\frac{2\pi x}{c}\sin\theta_p+\frac{\pi d\sin\theta_p\left(M-1\right)}{c}\right]\end{aligned}\tag{21}$$

When $\theta_p \neq 0°$, the phase difference $\Delta_{u,v}$ is a function of the phase center location of the array x. Therefore, the value of $\left|\sum_{q=1}^{Q}\boldsymbol{a}^H\left(\theta_p, f_q\right)\boldsymbol{a}\left(\theta, f\right)\right|$ depends on the phase center location of the array x.

Now consider the influence of complex weighted vector $\boldsymbol{V}$. According to the solution procedure of complex weighted vector $\boldsymbol{V}$,

$$\begin{cases}\boldsymbol{g}=\boldsymbol{C}\boldsymbol{V}\\ \boldsymbol{C}^H\boldsymbol{g}=\boldsymbol{F}\end{cases}\Rightarrow\boldsymbol{V}=\left(\boldsymbol{C}^H\boldsymbol{C}\right)^{-1}\boldsymbol{F}\tag{22}$$

it can be found that the complex weighted vector $\boldsymbol{V}$ can only control the array response of the preselected points to meet the unit gain, but can not control the array response in other directions and frequencies outside the preselected points. Therefore, in addition to the unit gain of the preselected points, the values of $P\left(\theta, f\right)$ will depend on the phase center location of the array x.

Remarks 1: When $\theta_p = 0°$, the phase center location of the array x does not affect the calculation results in (18)(19)(21), so the quiescent beam response is not affected by the phase center location of the array x.

This concludes the proof.

Theoretical derivation proves the accuracy of the dependence between the stationary beam response and the phase center of the array. In order to further understand the impact of the array phase center on the quiescent beam response of FCSTBB, the following numerical simulation is designed.

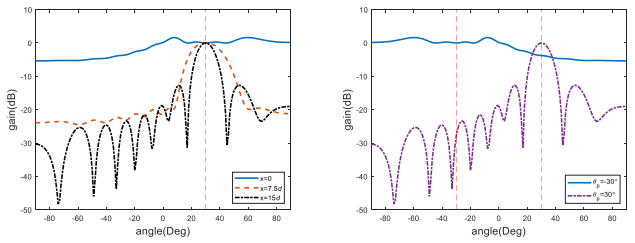

(a) (b)

FIGURE 4. Quiescent beam pattern: (a) different array phase center position; (b) different desired wave directions.

Firstly, Fig. 4(a) simulates the quiescent beam pattern for three different phase center locations of the array $x = 0, 7.5d, 15d$. The sampling frequency f_s used is equal to two times the maximum array frequency, the signal processing bandwidth is extended from $0.2f_s$ to $0.4f_s$. $M = 16, L = 11, \theta_p = 30°$, and $Q = 21$ were selected in simulation. The quiescent beam pattern only shows the beam response at $f = 0.3f_s$. As shown in Fig. 4(a), the beam pattern at $x = 0$ has serious distortion, the sidelobe level is significantly higher than the other two beam patterns, and it is difficult to distinguish the location of the main lobe of the beam pattern. The main lobe width and sidelobe level of the beam pattern at $x = 7.5d$ have been greatly improved compared to $x = 0$, but the beam pattern at $x = 15d$ has narrower main lobe width and lower sidelobe level. Therefore, the phase center of the array has a significant influence on the quiescent beam response, and there is an optimal phase center of the array, which makes the beamformer get the best beam response.

Secondly, Fig. 4(b) simulates the quiescent beam pattern of a set of desired signals with symmetric incoming wave direction ($\theta_p = -30°, 30°$) at the same phase center location of the array $x = 15d$, respectively. As shown in Fig. 4(b), when the array phase center is selected as $x = 15d$, although a better quiescent beam response is obtained when $\theta_p = 30°$, the beam pattern is seriously distorted when $\theta_p = -30°$. At the same phase center location of the array, selecting a different incoming direction θ_p of the desired signal will cause a significant change in the quiescent beam response. Therefore, different phase center locations of the array should be selected for different desired wave directions.

IV. OPTIMAL ARRAY PHASE CENTER

In order to quantify the optimal phase center of the array for the optimal beam response of the FCSTBB, it is necessary to select an evaluation n index to establish the variable relationship between the best beam response and the array phase center. three commonly used evaluation indices of beam response are considered to apply to the theoretical design criteria of optimal beam response: the main lobe width and sidelobe level of the beam pattern, the output signal to interference and noise ratio (SINR) and the quiescent output power of the array under white noise input.

First of all, due to the lack of quantitative criteria, the main lobe width and side lobe level of beam response can not be used as a theoretical design criterion. Second, The output SINR of the beamformer can be expressed as

$$\begin{aligned}SINR&=\frac{\boldsymbol{w}_{opt}^H\boldsymbol{R}_s\boldsymbol{w}_{opt}}{\boldsymbol{w}_{opt}^H\left(\sigma_n^2\boldsymbol{I}+\boldsymbol{R}_i\right)\boldsymbol{w}_{opt}}\\&=\frac{\sigma_s^2}{\left(\boldsymbol{g}+\bar{\boldsymbol{w}}\right)^H\left(\sigma_n^2\boldsymbol{I}+\boldsymbol{R}_i\right)\left(\boldsymbol{g}+\bar{\boldsymbol{w}}\right)}\end{aligned}\tag{23}$$

where $\boldsymbol{R}_s$ and $\boldsymbol{R}_i$ represent the space-time covariance matrix of the desired signal and the space-time covariance matrix of the interference, respectively. σ_s^2 and σ_n^2 respectively represent the power of the desired signal and the power of white noise. Because the solution vector $\bar{\boldsymbol{w}}$ is a function of the inverse matrix of data covariance, the relationship between SINR and the location of the phase center is highly nonlinear and depends on the location of interference. Therefore, SINR

can not be used as a theoretical design criterion. Finally, Considering the quiescent condition without interference, the output SNR of the beamformer can be calculated as

$$\mathrm{SNR} = \frac{\sigma_s^2}{\sigma_n^2 \boldsymbol{g}^H \boldsymbol{g}} \tag{24}$$

where $\sigma_n^2 \boldsymbol{g}^H \boldsymbol{g}$ represents the quiescent output power of the array under white noise input. It can be found that minimizing the quiescent output power is equivalent to maximizing the output SNR. Therefore, the quiescent output power of the array can be selected as the evaluation index of the design criterion for the best quiescent beam response. The optimal phase center of the array should minimize the quiescent output power of the array.

Under white noise input, the theoretical equation of the quiescent output power of the array is

$$\begin{aligned} P_n &= \sigma_n^2 \boldsymbol{g}^H \boldsymbol{g} \\ &= \sigma_n^2 \boldsymbol{F}^H \left(\boldsymbol{C}^H \boldsymbol{C} \right)^{-1} \boldsymbol{F} \end{aligned} \tag{25}$$

in which the constraint matrix $\boldsymbol{C}$ and the response vector $\boldsymbol{F}$ are given by (15) and (16), respectively. σ_n^2 is the white noise power. In order to obtain the functional relationship between the quiescent output power of the array and the phase center of the array, it is necessary to expand (25) for theoretical derivation. However, when the order of $\boldsymbol{C}^H \boldsymbol{C}$ is greater than two, the expansion of its inverse matrix is complicated. Theoretically, the functional relationship between the quiescent output power of the array and the phase center of the array can only be obtained when the constraint matrix $\boldsymbol{C}$ contains two preselected points.

A. THE CLOSED-FORM SOLUTION OF THE OPTIMAL PHASE CENTER LOCATION WHEN THE CONSTRAINT MATRIX CONTAINS TWO PRESELECTED POINTS

Considering the constraint matrix contains two preselected points, their desired wave directions are θ_p, and the frequencies are f_u and f_v, respectively. The corresponding constraint matrix $\boldsymbol{C'}$ and response vector $\boldsymbol{F'}$ can be obtained as follows

$$\begin{cases} \boldsymbol{C'} = \left[\boldsymbol{a}\left(\theta_p, f_u\right), \boldsymbol{a}\left(\theta_p, f_v\right) \right] \\ \boldsymbol{F'} = [1, 1] \end{cases} \tag{26}$$

Substitute (26) into (25), expand the inverse matrix of $\boldsymbol{C'}$ and simplify the result, we obtain

$$P_n = \sigma_n^2 \frac{2ML - 2\left| \boldsymbol{a}^H\left(\theta_p, f_u\right) \boldsymbol{a}\left(\theta_p, f_v\right) \right| \cos \Phi_{u,v}}{(ML)^2 - \left| \boldsymbol{a}^H\left(\theta_p, f_u\right) \boldsymbol{a}\left(\theta_p, f_v\right) \right|^2} \tag{27}$$

where

$$\Phi_{u,v} = \Phi\left[\boldsymbol{a}^H\left(\theta_p, f_u\right) \boldsymbol{a}\left(\theta_p, f_v\right) \right] \tag{28}$$

Calculate $\boldsymbol{a}^H\left(\theta_p, f_u\right) \boldsymbol{a}\left(\theta_p, f_v\right)$ according to (19)(20), where (20) can be rewritten as

$$\begin{cases} \varphi_t = \dfrac{2\pi}{f_s}\left(f_v - f_u\right) \\ \varphi_0 = -\dfrac{x}{d}\alpha\left(\sin\theta_p\right)\varphi_t \\ \varphi_s = \alpha\left(\sin\theta_p\right)\varphi_t \end{cases} \tag{29}$$

where $\alpha = f_s/\left(2f_0\right)$, and f_0 is the maximum frequency of the array. Substituting (29) into (19), we obtain

$$\begin{aligned} &\boldsymbol{a}^H\left(\theta_p, f_u\right) \boldsymbol{a}\left(\theta_p, f_v\right) \\ &= \frac{\sin\left(L\varphi_t/2\right)}{\sin\left(\varphi_t/2\right)} \frac{\sin\left(M\varphi_s/2\right)}{\sin\left(\varphi_s/2\right)} e^{-j\varphi_t\left[\frac{L-1}{2} + \left(\alpha\sin\theta_p\right)\left(\frac{M-1}{2} - \frac{x}{d}\right)\right]} \end{aligned} \tag{30}$$

When $\theta_p \neq 0°$, the array quiescent output power P_n is a multivariate function as follows.

$$P_n = \mathrm{P}\left(f_v - f_u, \alpha\sin\theta_p, x\right) \tag{31}$$

The minimum value of P_n about the phase center location x of the array satisfies the following expression

$$\begin{cases} \dfrac{\partial P_n}{\partial x} = 0 \\ \dfrac{\partial^2 P_n}{\partial x^2} > 0 \end{cases} \tag{32}$$

Combining (27)(29)(30) to calculate (32). When the array quiescent output power P_n takes the minimum value, the phase center location of the array x satisfies the following expression

$$\Phi_{u,v} = -\varphi_t\left[\frac{L-1}{2} + \left(\alpha\sin\theta_p\right)\left(\frac{M-1}{2} - \frac{x}{d}\right)\right] = 2k\pi \quad (k = 0, \pm1, \pm2, \ldots) \tag{33}$$

Substituting (33) into (27), it is easy to find that the minimum values of P_n are the same. Therefore, when the constraint matrix contains two preselected points, all x satisfying (33) are the optimal phase center location of the array. When the constraint matrix contains two preselected points, the closed-form solution of the optimal phase center location of the array can be calculated by the following equation

$$x_{opt,2point} = \left[\frac{kf_s}{\left(f_v - f_u\right)\alpha\sin\theta_p} + \frac{L-1}{2\alpha\sin\theta_p} + \frac{M-1}{2}\right] d \quad \left(\theta_p \neq 0, k = 0, \pm1, \pm2, \ldots\right) \tag{34}$$

At $\theta_p = 0°$, $\sin\theta_p = 0$ makes the array output power P_n independent of the phase center location of the array x.

B. SUBOPTIMAL SOLUTION OF OPTIMAL PHASE CENTER LOCATION

Due to the inverse of the matrix exceeding the two orders can not be expanded, the closed-form solution of the optimal phase center location of the array can not be solved when the constraint matrix contains more than two preselected points.

Extrapolate (34) to obtain the suboptimal solution for the optimal phase center location may be a good solution.

Substituting (33) into (30), the inner product between the space-time steering vectors of two preselected points is a real number at the optimal phase center of the array. According to (25), the quiescent output power of the array depends on $\boldsymbol{C}^H\boldsymbol{C}$, Substitute (15) into $\boldsymbol{C}^H\boldsymbol{C}$, we get

$$\boldsymbol{C}^H\boldsymbol{C} = \begin{bmatrix} \boldsymbol{a}_1^H\boldsymbol{a}_1 & \boldsymbol{a}_1^H\boldsymbol{a}_2 & \cdots & \boldsymbol{a}_1^H\boldsymbol{a}_Q \\ \boldsymbol{a}_2^H\boldsymbol{a}_1 & \boldsymbol{a}_2^H\boldsymbol{a}_2 & \cdots & \boldsymbol{a}_2^H\boldsymbol{a}_Q \\ \vdots & \vdots & \ddots & \vdots \\ \boldsymbol{a}_Q^H\boldsymbol{a}_1 & \boldsymbol{a}_Q^H\boldsymbol{a}_2 & \cdots & \boldsymbol{a}_Q^H\boldsymbol{a}_Q \end{bmatrix} \tag{35}$$

where $\boldsymbol{a}_q = \boldsymbol{a}\left(\theta_p, f_q\right) q = 1, 2, \ldots, Q$. Therefore, the quiescent output power of the array depends on the inner product of the space-time steering vectors. Based on the above conclusions, an easy extrapolation conclusion is that the expected suboptimal solution of the optimal array phase center should ensure that the inner product of the space-time steering vectors of any two preselected points in the constraint matrix is a real number.

Next, based on the closed solution (34), the suboptimal solution of the optimal array phase center is found. At $k \neq 0$, $x_{opt,2point}\ (k \neq 0)$ depends on the frequency interval between the two preselected points. Therefore, when the constraint matrix contains more than two preselected points, the phase center location of the array $x_{opt,2point}\ (k \neq 0)$ can not guarantee that the inner product between the space-time steering vectors corresponding to any two preselected points is a real number. At $k = 0$,

$$x_{opt,2point}\ (k = 0) = \left[\frac{L-1}{2\alpha \sin\theta_p} + \frac{M-1}{2}\right] d\left(\theta_p \neq 0\right) \tag{36}$$

(36) is an exciting result, which not only makes the optimal phase center location independent of the frequency of the preselected points when the constraint matrix $\boldsymbol{C}$ contains two preselected points, but also makes the inner product of the space-time steering vectors corresponding to any two preselected points in constraint matrix $\boldsymbol{C}$ real when the constraint matrix $\boldsymbol{C}$ contains more than two preselected points. This unique ability of (36) indicates that when the constraint matrix $\boldsymbol{C}$ contains more than two preselected points, it may be the suboptimal solution to the optimal phase center location of the array. Proving this extrapolation by theoretical derivation requires expanding $\left(\boldsymbol{C}^H\boldsymbol{C}\right)^{-1}$, which is a complex and difficult task. However, (36) is a reasonable extrapolation result based on the existing conditions, which provides a quick method to solve the optimal phase center location of the array when the constraint matrix contains any number of preselected points. Otherwise, solving the optimal phase center location of the array can only search the phase center of the array where the minimum quiescent output power of the array lies inefficiently. The effectiveness of this extrapolated suboptimal solution will be verified by numerical simulation in the next section.

V. SIMULATION RESULTS

In this section, the correctness and effectiveness of the closed-form solution (34) and the suboptimal solution (36) of the optimal phase center location are verified by numerical simulation. The influence of the frequency interval Δf between the preselected points and the filter tap number L on the dependence of the phase center of the array on the quiescent beam response is simulated and analyzed. Consider a 16-element ($M = 16$) ULA, using tapped delay lines with eleven taps ($L = 11$) at each element. Assuming that it works in a broadband environment, the element spacing is equal to half the wavelength of the maximum frequency component. Use a sampling frequency f_s equal to two times the maximum frequency and extend the useful source bandwidth from $0.2f_s$ to $0.4f_s$.

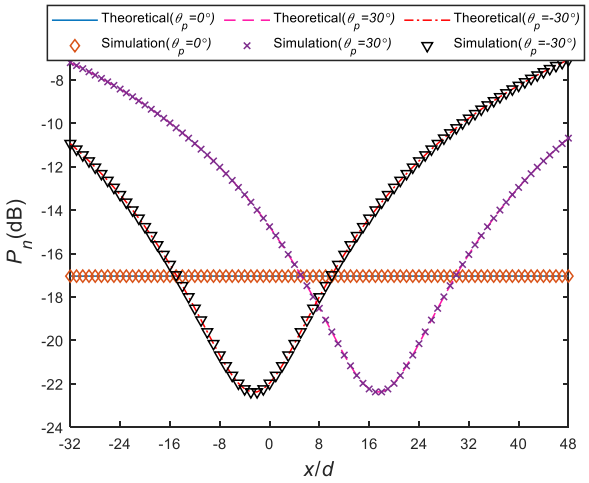

FIGURE 5. Theoretical and simulated values of array quiescent output power versus different array phase center positions under different desired directions.

A. COMPARISON OF THEORETICAL AND SIMULATED VALUES

Fig. 5 indicates the theoretical and simulated values of the array quiescent output power versus different phase center locations of the array when the constraint matrix contains two preselected points. The theoretical value is calculated according to (27) derived from (25), and the simulated value (25) is directly calculated by computer. In the simulation, the two preselected points are $\left(\theta_p, 0.3f_s\right)$ and $\left(\theta_p, 0.31f_s\right)$. The desired signal direction θ_p is selected from three representative directions $\theta_p = -30°, 0°, 30°$ for three times of simulation. Fig. 5 reveals that the theoretical value is completely consistent with the simulation value. It proves the correctness of the closed-form solution (34). In addition, when the optimal phase center location of the array at $\theta_p = 30°$ is applied to $\theta_p = -30°$, the output power of the array is increased by about 8 dB, which indicates that different desired directions θ_p should correspond to different optimal phase center locations of the array.

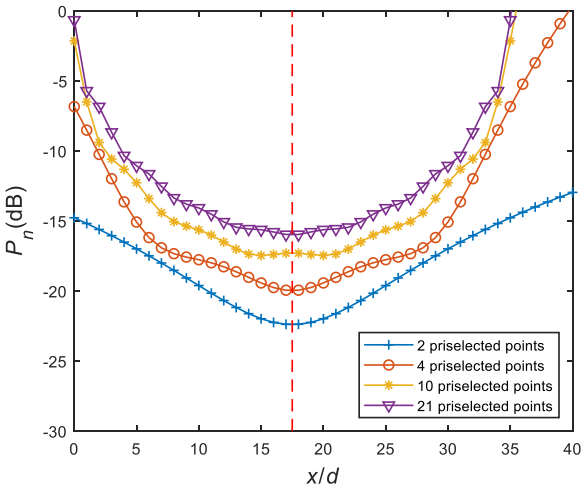

FIGURE 6. The array quiescent output power versus different array phase center positions under different number of preselected points.

TABLE 1. Simulation parameters.

The number of preselected points	θ_p	f_q
2	30°	$0.3f_s$: $0.01f_s$: $0.31f_s$
4	30°	$0.29f_s$: $0.01f_s$: $0.32f_s$
10	30°	$0.26f_s$: $0.01f_s$: $0.35f_s$
21	30°	$0.2f_s$: $0.01f_s$: $0.4f_s$

B. OPTIMAL PHASE CENTER LOCATION OF THE ARRAY WHEN CONSTRAINED MATRIX CONTAINS DIFFERENT NUMBERS OF PRESELECTED POINTS

Fig. 6 compares the curves of quiescent output power of the array versus the different phase center location of the array x when the constraint matrix contains different numbers of preselected points. Select simulation parameters of preselected points according to Table 1. As shown in Fig. 6, the abscissa of the bottom center location of all four groups of quiescent output power curves is 17.5d, which is consistent with suboptimal solution that the optimal phase center location $x_{opt,2point}$ $(k = 0) = 17.5d$ calculated according to (36). When the number of preselected points are 2,4,21, the bottom center location of the change curve is also the minimum. When the number of preselected points is 10, although the variation curve does not get the minimum value at 17.5d, the difference is very small compared to the minimum value. The slight difference indicates that the performance difference between the quiescent beam response of the array phase center selection of 17.5d and the real minimum value selection is almost negligible. Because it is difficult to solve the phase center location of the array where the real minimum value is located, (36) can be used as a suboptimal selection of the optimal phase center location of the array. Therefore, when the constraint matrix contains any number of preselected points, the phase center location of the array obtained from (36) can be used as the suboptimal solution of the optimal phase center location of the array.

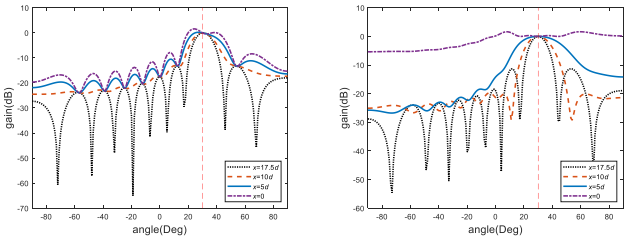

FIGURE 7. Quiescent beam pattern versus different array quiescent output power: (a) 2 preselected points; (b) 21 preselected points.

TABLE 2. The relationship between the array quiescent output power and the array phase center.

Array phase center x	Quiescent output power (2 preselected points) (dB)	Quiescent output power (21 preselected points) (dB)
$17.5d$	-22.37	-15.96
$10d$	-19.61	-14.07
$5d$	-16.98	-11.05
0	-14.77	-0.64

C. QUIESCENT BEAM PATTERN UNDER DIFFERENT ARRAY QUIESCENT OUTPUT POWER

When the constraint matrix contains two preselected points, the quiescent beam pattern at different quiescent output power of the array is shown in Fig. 7(a). Fig. 7(b) demonstrates that the quiescent beam pattern under different quiescent output powers of the array when the constraint matrix contains 21 preselected points. The quiescent beam pattern only reveals the beam response when $f = 0.3f_s$. By selecting different phase center locations of the array, the quiescent beam patterns under different quiescent output powers of the array can be obtained. The corresponding relationship between the array quiescent output power and the array phase center is presented in Table 2. It can be seen from Fig. 7(a) that when the quiescent output power of the array takes the minimum value, the quiescent beam pattern can obtain the narrowest main lobe width and the lowest sidelobe level. In addition, it is obvious that the greater the difference between the quiescent output power of the array and the theoretical minimum output power, the worse the performance of the corresponding quiescent beam response. The simulation results of Fig. 7(b) are similar to that of Fig. 7(a), indicating that when the constraint matrix contains more than two preselected points, the suboptimal solution (33) of the optimal phase center of the array can make the quiescent output power of the array minimum or approximately minimum.

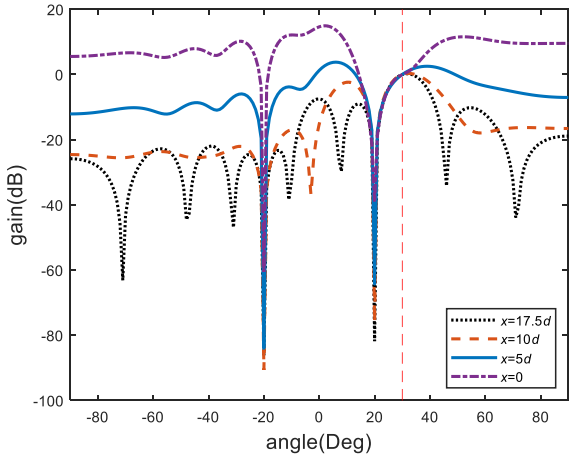

FIGURE 8. Optimal beam pattern versus different array phase centers.

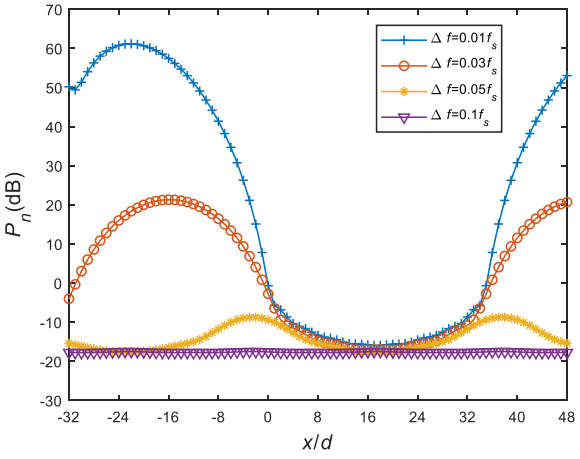

FIGURE 9. The array quiescent output power versus different array phase center positions under different preselected point frequency intervals.

D. OPTIMAL BEAM PATTERN UNDER DIFFERENT ARRAY PHASE CENTERS

The optimal beam patterns of FCSTBB under different phase centers of the array are shown in Fig. 8. The wave directions of the broadband main lobe interference source, the broadband side lobe interference source and the broadband desired source are 20°, −20° and 30°, respectively. The constraint matrix of the beamformer contains 21 preselected points, and the parameters of the preselected points are selected according to Table 1. The phase center locations of the array are chosen as 0, $5d$, $10d$, and $17.5d$, respectively. Table 3 lists the null depth of the interference direction in the optimal beam pattern. In Fig. 8, when the optimal phase center location is selected, the beamformer can obtain the narrowest main lobe width and the lowest sidelobe level while forming interference nulling. When the other three array phase centers are selected, the main lobe width and the side lobe level are increased to varying degrees. Table 3 indicates that the selection of the phase center location of the array will affect the beampattern null depth. Among them, the widening of the main lobe and the increase of the sidelobe level caused by the improper selection of the array phase center will reduce the depth of main lobe interference nulling and side lobe interference nulling, respectively.

TABLE 3. Optimal beam pattern null depth.

Array phase center x	Null depth (dB)	
	-20°	20°
$17.5d$	-86.11	-81.8
$10d$	-90.64	-75.9
$5d$	-83.99	-64.29
0	-60.51	-39.12

E. EFFECT OF PRESELECTED POINT FREQUENCY INTERVALS

The variation of the array quiescent output power with the phase center location of the array x at different frequency intervals of the preselected point Δf is given in Fig. 9. Considering the useful source bandwidth $[0.2f_s, 0.4f_s]$, four groups of preselected points are selected with different frequency intervals $\Delta f = 0.01f_s, 0.03f_s, 0.05f_s, 0.1f_s$ respectively. Fig. 9 reveals that the difference between the maximum and minimum values of the array quiescent output power decreases with the increase of the frequency interval Δf of the preselected points. The phase centers of the array with the maximum and minimum of the quiescent output power correspond to the worst and best quiescent beam response performance, respectively. Therefore, the difference between the maximum and the minimum value of the simulation curve can reflect the dependence of the quiescent beam response on the phase center location of the array. For the three simulation curves $\Delta f = 0.01f_s, 0.03f_s, 0.05f_s$, the phase center location of the array x still has a great influence on the quiescent output power, so the dependence of the array phase center on the quiescent beam response can not be ignored. However, for $\Delta f = 0.1f_s$, the output power of the array hardly changes with the phase center location of the array x, so this dependence can be ignored. Although the number of preselected points in each group is different in the simulation, the simulation results in Fig.6 demonstrate that reducing the number of preselected points will not make the dependence of the array phase center on the quiescent beam response negligible.

F. EFFECT OF FILTER TAP NUMBER

Fig. 10 shows the variation of the quiescent output power of the array with the phase center location x under different filter taps L. Five filter taps $L = 11,31,51,81,101$ are considered. The constraint matrix of the beamformer contains 21 preselected points, and the parameters of the preselected points are selected according to Table 1. As is clear from Fig 10, with the increase of filter taps L, the difference between the maximum and minimum values in the simulation curve decreases, that is, the dependence of the quiescent beam response on the phase center location of the array

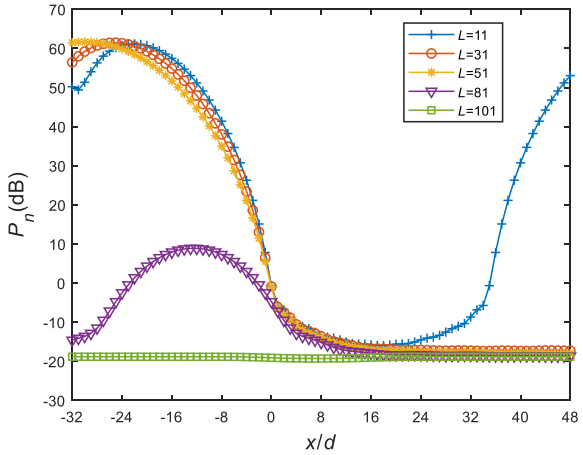

FIGURE 10. The array quiescent output power versus different array phase center positions under different filter tap numbers.

decreases. When the number of filter taps is chosen $L = 101$, the output power of the array hardlychanges with the phase center location of the array x, so the dependence of the phase center of the array on the quiescent beam response can be neglected.

VI. CONCLUSION

In this paper, the dependence of the quiescent beam response of the FCSTBB on the array phase center is pointed out, and the accuracy of this dependence is proved by theoretical derivation and numerical simulation. In order to solve the optimal phase center location of the array, minimizing the quiescent output power of the array under the input of white noise is selected as the selection criterion of the optimal phase center location of the array. Then, through theoretical derivation, the closed-form solution of the optimal phase center location of the array is obtained when the linear constraint contains two preselected points. Since the inverse of the high-order matrix can not be derived theoretically, the closed-form solution of the optimal phase center location of the array when the constraint matrix contains more than two preselected points can not be given. In order to solve this problem, based on the derived closed-form solution, a suboptimal solution of the optimal phase center location of the array is correctly derived when the linear constraint contains any number of preselected points. The numerical simulations indicate that the suboptimal solution can make the beam pattern of FCSTBB obtain the narrowest main lobe width and the lowest side lobe level, and at the same time improve the depth of null.

In addition, the influence of the frequency interval of the preselected points and the number of filter taps on the dependence of the quiescent beam response on the array phase center is simulated and analyzed. The results show that when the selected preselected point frequency interval Δf or the number of filter taps L is large enough, the dependence of the quiescent beam response on the phase center location of the array can be ignored. The research in this paper is helpful in the selection of the optimal phase center location of the ULA in FCSTBB.

REFERENCES

[1] J. Li, Z. Ma, L. Mao, Z. Wang, Y. Wang, H. Cai, and X. Chen, "Broadband generalized sidelobe canceler beamforming applied to ultrasonic imaging," *Appl. Sci.*, vol. 10, no. 4, p. 1207, Feb. 2020.
[2] G. Zhou, "Energy efficiency beamforming design for UAV communications with broadband hybrid polarization antenna arrays," *IEEE Access*, vol. 7, pp. 34521–34532, 2019.
[3] X. Wang, I. Cohen, J. Chen, and J. Benesty, "On robust and high directive beamforming with small-spacing microphone arrays for scattered sources," *IEEE/ACM Trans. Audio, Speech, Language Process.*, vol. 27, no. 4, pp. 842–852, Apr. 2019.
[4] J. Qiu, Z. Li, X. Jin, X. Yu, S. Zheng, and X. Zhang, "Long distance broadband fiber optical beamforming over 120 km," *IEEE Access*, vol. 9, pp. 152182–152187, 2021.
[5] Y. Wang, Y. Yang, Y. Ma, Z. He, and Y. Liu, "Broadband pattern synthesis for circular sensor arrays," *J. Acoust. Soc. Amer.*, vol. 136, no. 2, pp. EL153–EL158, Aug. 2014.
[6] B. D. Van Veen and K. M. Buckley, "Beamforming: A versatile approach to spatial filtering," *IEEE ASSP Mag.*, vol. M-5, no. 2, pp. 4–24, Apr. 1988.
[7] W. Liu and S. Weiss, *Wideband Beamforming: Concepts and Techniques*. Hoboken, NJ, USA: Wiley, 2010.
[8] L. Griffiths and K. Buckley, "Quiescent pattern control in linearly constrained adaptive arrays," *IEEE Trans. Acoust., Speech, Signal Process.*, vol. ASSP-35, no. 7, pp. 917–926, Jul. 1987.
[9] F. Liu, R. Du, J. Wu, Q. Zhou, Z. Zhang, and Y. Cheng, "Multiple constrained l_2-norm minimization algorithm for adaptive beamforming," *IEEE Sensors J.*, vol. 18, no. 15, pp. 6311–6318, Aug. 2018.
[10] S. Yan, "Optimal design of FIR beamformer with frequency invariant patterns," *Appl. Acoust.*, vol. 67, no. 6, pp. 511–528, 2006.
[11] Y. Wang, Y. Yang, G. Jiang, and K. Fan, "Optimal design of frequency-invariant beamformers for circular arrays," in *Proc. OCEANS MTS/IEEE*, Oct. 2018, pp. 1–5.
[12] L. C. Godara, "Application of the fast Fourier transform to broadband beamforming," *J. Acoust. Soc. Amer.*, vol. 98, no. 1, pp. 230–240, Jul. 1995.
[13] S. Zhang, J. Thiyagalingam, W. Sheng, T. Kirubarajan, and X. Ma, "Low-complexity adaptive broadband beamforming based on the non-uniform decomposition method," *Signal Process.*, vol. 151, pp. 66–75, Oct. 2018.
[14] X. Yang, S. Li, Q. Liu, T. Long, and T. K. Sarkar, "Robust wideband adaptive beamforming based on focusing transformation and steering vector compensation," *IEEE Antennas Wireless Propag. Lett.*, vol. 19, no. 12, pp. 2280–2284, Dec. 2020.
[15] R. T. Compton Jr., "The relationship between tapped delay-line and FFT processing in adaptive arrays," *IEEE Trans. Antennas Propag.*, vol. AP-36, no. 1, pp. 15–26, Jan. 1988.
[16] O. L. Frost, "An algorithm for linearly constrained adaptive array processing," *Proc. IEEE*, vol. 60, no. 8, pp. 926–935, Aug. 1972.
[17] J. Dmochowski, J. Benesty, and S. Affes, "Linearly constrained minimum variance source localization and spectral estimation," *IEEE Trans. Audio, Speech, Language Process.*, vol. 16, no. 8, pp. 1490–1502, Nov. 2008.
[18] Z. Liu, S. Zhao, G. Zhang, and B. Jiao, "Robust adaptive beamforming for sidelobe canceller with null widening," *IEEE Sensors J.*, vol. 19, no. 23, pp. 11213–11220, Dec. 2019.
[19] M. Zhang, X. Wang, and A. Zhang, "An efficient broadband adaptive beamformer without presteering delays," *Sensors*, vol. 21, no. 4, p. 1100, Feb. 2021.
[20] S. Zhang, Q. Gu, H. Sun, W. Sheng, and T. Kirubarajan, "Adaptive broadband frequency invariant beamforming using nulling-broadening and frequency constraints," *Signal Process.*, vol. 195, Jun. 2022, Art. no. 108461.
[21] S. Zhang and I. L. J. Thng, "Robust presteering derivative constraints for broadband antenna arrays," *IEEE Trans. Signal Process.*, vol. 50, no. 1, pp. 1–10, Jan. 2002.
[22] K. Buckley, "Spatial/spectral filtering with linearly constrained minimum variance beamformers," *IEEE Trans. Acoust., Speech, Signal Process.*, vol. ASSP-35, no. 3, pp. 249–266, Mar. 1987.
[23] L. C. Godara and M. R. S. Jahromi, "Convolution constraints for broadband antenna arrays," *IEEE Trans. Antennas Propag.*, vol. 55, no. 11, pp. 3146–3154, Nov. 2007.

[24] R. Ebrahimi and S. R. Seydnejad, "Elimination of pre-steering delays in space-time broadband beamforming using frequency domain constraints," *IEEE Commun. Lett.*, vol. 17, no. 4, pp. 769–772, Apr. 2013.
[25] K. M. Buckley and L. J. Griffiths, "Linearly-constrained beamforming: A relationship between phase center location and beampattern," in *Proc. 19th Asilomar Conf. Circuits, Syst. Comput.*, 1985, pp. 234–238.
[26] K. M. Buckley and L. J. Griffiths, "An adaptive generalized sidelobe canceller with derivative constraints," *IEEE Trans. Antennas Propag.*, vol. AP-34, no. 3, pp. 311–319, Mar. 1986.
[27] C.-C. Tseng, "Minimum variance beamforming with phase-independent derivative constraints," *IEEE Trans. Antennas Propag.*, vol. 40, no. 3, pp. 285–294, Mar. 1992.
[28] C.-Y. Tseng and L. J. Griffiths, "Adaptive broadband beamforming using phase-independent derivative constraint techniques," in *Proc. IEEE Int. Conf. Acoust. Speech Signal Process.*, Apr. 1993, pp. 536–539.

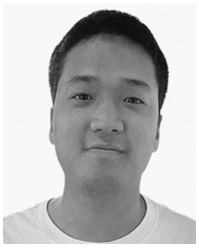

YANG WANG was born in 1996. He received the B.S. degree from Harbin Engineering University, in 2020. He is currently pursuing the M.S. degree with PLA Strategic Support Force Information Engineering University. His research interests include array signal processing and sonar signal processing.

HAIYUN XU received the M.S. and Ph.D. degrees from the National Digital Switching System Engineering and Technological Research Center (NDSC), Zhengzhou, China, in June 2019 and June 2022, respectively. He is currently working in communications and information system with PLA Strategic Support Force Information Engineering University. His research interests include the areas of array signal processing and parameter estimation.

BIN WANG received the Ph.D. degree from Information Engineering University, in 2007. She is currently an Associate Professor with the School. Her research interests include underwater acoustic communication, signal processing, and blind channel equalization.

MINGLEI SUN received the Ph.D. degree from the Harbin Institute of Technology, in 2015. He is currently with PLA Strategic Support Force Information Engineering University. His research interest includes array signal processing.